Structural characterization of mRNA-tRNA translocation intermediates

Xabier Agirrezabala[a,1], Hstau Y. Liao[b,1], Eduard Schreiner[c,d,2], Jie Fu[b], Rodrigo F. Ortiz-Meoz[e], Klaus Schulten[c,d,f], Rachel Green[e], and Joachim Frank[b,g,3]

[a]Structural Biology Unit, CIC-bioGUNE, Bizkaia Technology Park, Derio 48160, Basque Country, Spain; [b]Howard Hughes Medical Institute, Department of Biochemistry and Molecular Biophysics, Columbia University, 630 168th Street, P&S BB 2-221, New York, NY; [c]Beckman Institute for Advanced Science and Technology, [d]Center for Biophysics and Computational Biology, University of Illinois at Urbana-Champaign, Urbana, IL; [e]Howard Hughes Medical Institute, Department of Molecular Biology and Genetics, Johns Hopkins University School of Medicine, Baltimore, MD 21205; [f]Department of Physics, University of Illinois at Urbana-Champaign, Urbana, IL; and [g]Department of Biological Sciences, Columbia University, New York, NY

Contributed by Joachim Frank, January 31, 2012 (sent for review November 21, 2011)

Cryo-EM analysis of a wild-type *Escherichia coli* pretranslocational sample has revealed the presence of previously unseen intermediate substates of the bacterial ribosome during the first phase of translocation, characterized by intermediate intersubunit rotations, L1 stalk positions, and tRNA configurations. Furthermore, we describe the domain rearrangements in quantitative terms, which has allowed us to characterize the processivity and coordination of the conformational reorganization of the ribosome, along with the associated changes in tRNA ribosome-binding configuration. The results are consistent with the view of the ribosome as a molecular machine employing Brownian motion to reach a functionally productive state via a series of substates with incremental changes in conformation.

cryo-EM | E. coli | ribosome | translation

Changes in ribosome conformation during protein synthesis are substantial, the most pronounced ones occurring during mRNA-tRNA translocation along the A (aminoacyl), P (peptidyl), and E (exit) tRNA binding sites of the ribosome, as postulated early on by Spirin (1) and Bretscher (2) and shown in recent studies by cryo-EM, X-ray crystallography, and smFRET [see (3)]. These changes go along with changes in binding configurations the ribosome forms with the tRNAs and elongation factor G (EF-G) in the process of translocation.

Translocation can be broadly divided into two phases [see (4)]: during the first phase, the tRNAs move with respect to the large (50S) subunit, and in the second, the mRNA and the tRNAs affixed to it move with respect to the small (30S) subunit. After accommodation of the incoming aminoacyl-tRNA into the A/A site, and peptide transfer from the peptidyl-tRNA residing in the P/P site, the tRNAs proceed from the classical (A/A, P/P) to the hybrid (A/P, P/E) binding configuration (5): while the anticodon stem loops (ASLs) of tRNAs stay in the small subunit's A and P sites, the acceptor ends move to the large subunit's P and E sites, respectively. As EF-G binds to the complex, the ribosome undergoes a ratchet-like motion ("intersubunit rotation")—the 30S subunit rotates with respect to the 50S subunit (6). This rotation is accompanied by a movement of the L1 stalk of the 50S subunit toward the main body of the ribosome and a rotation of the head domain of the 30S subunit around its long axis (7–10). These movements separate two distinct states during the first phase of translocation, termed macrostate I (MS I) and II (MS II) (4). The fact that the conformational changes of the ribosome and classical-hybrid transitions of tRNAs occur spontaneously in a pretrans-locational (PRE) ribosome (11–16) has confirmed the view of the ribosome as a Brownian machine (17). In this view, the role of ribosomal factors is to modulate the free-energy landscape, promoting or controlling structural and kinetic routes underlying functional dynamics of translation (18, 19). In the case of translocation, smFRET has provided rich detail on the way EF-G promotes and controls the reaction [e.g., (13, 14, 20–27)].

Cryo-EM (11, 15) of factor-free PRE WT *Escherichia coli* samples revealed a large structural reorganization of the ribosome and associated classical → hybrid changes of tRNA ribosome-binding configuration in going from MS I to MS II. The size of these changes made it very likely that structural intermediates exist. Evidence for such intermediates was found by smFRET (28), by cryo-EM of the back-translocation process (29), of the second phase of translocation (8), of ribosomes with a P-loop mutation (30), and by X-ray crystallography of 70S ribosomes with ASL mimics (31), prompting us to reexamine the WT *E. coli* PRE ribosome complex. We employed ML3D (32), a technique of maximum-likelihood based classification requiring no prior knowledge of the nature of the structural variability.

Results

Summary of Reconstructions. We applied ML3D to an existing dataset of the factor-free WT *E. coli* PRE complex (15), and obtained six classes. The class-1 reconstruction was discarded as it showed evidence for bias in particle orientations (see Fig. S1). Class 4 showed indications of residual heterogeneity, especially in the features of the tRNAs. Subsequent ML3D analysis subdivided this class into two more homogenous classes, bringing the total back to six. The outcome of the classification was evaluated by visual inspection and 3D variance analysis of the final six reconstructions (see Fig. S2).

Classes 2 (approximately 16%; see Fig. S3*A*) and 4A (10%; Fig. S3*C*) both correspond to ribosomes bearing classical A/A and P/P tRNAs. Class 3 (16%) corresponds to ribosomes bearing a single tRNA in the P site (Fig. S3*B*). Classes 4B (10%), 5 (17%), and 6 (18%) (Fig. S3 *D–F*, respectively) correspond to ribosomes that have undergone intersubunit rotation and bear hybrid-like tRNAs in A and P sites. The conformations of class-5 and -6 ribosomes are quite similar at the current resolution, and in turn similar to the one previously described as MS II (11, 15). (For a comparison of performance of the ML3D algorithm with that of the supervised approach, see Table S1).

Author contributions: X.A. and J. Frank designed research; X.A., H.Y.L, and E.S. performed research; R.F.O.-M. and R.G. contributed new reagents/analytic tools; X.A., H.Y.L., E.S., J. Fu, K.S., and J. Frank analyzed data; and X.A. and J. Frank wrote the paper.

The authors declare no conflict of interest.

Data deposition: The EM reconstructions were deposited in the 3D-EM database under the following accession numbers: EMD-5361, −5360, −5359, −5364, -5363, and −5362 for class 2, 3, 4A, 4B, 5, and 6, respectively. The atomic coordinates generated by MDFF were deposited with PDB ID codes 3J0U-3J0T, 3J13-3J11, 3J0V-3J0W, 3J0X-3J0Y, 3J0Z-3J12 and 3J10-3J14, for the small and large subunits, respectively.

[1]X.A. and H.L. contributed equally to the work.

[2]Present address: BASF SE, Materials Modeling, 67056 Ludwigshafen, Germany.

[3]To whom correspondence should be addressed. E-mail: jf2192@columbia.edu.

This article contains supporting information online at www.pnas.org/lookup/suppl/doi:10.1073/pnas.1201288109/-/DCSupplemental.

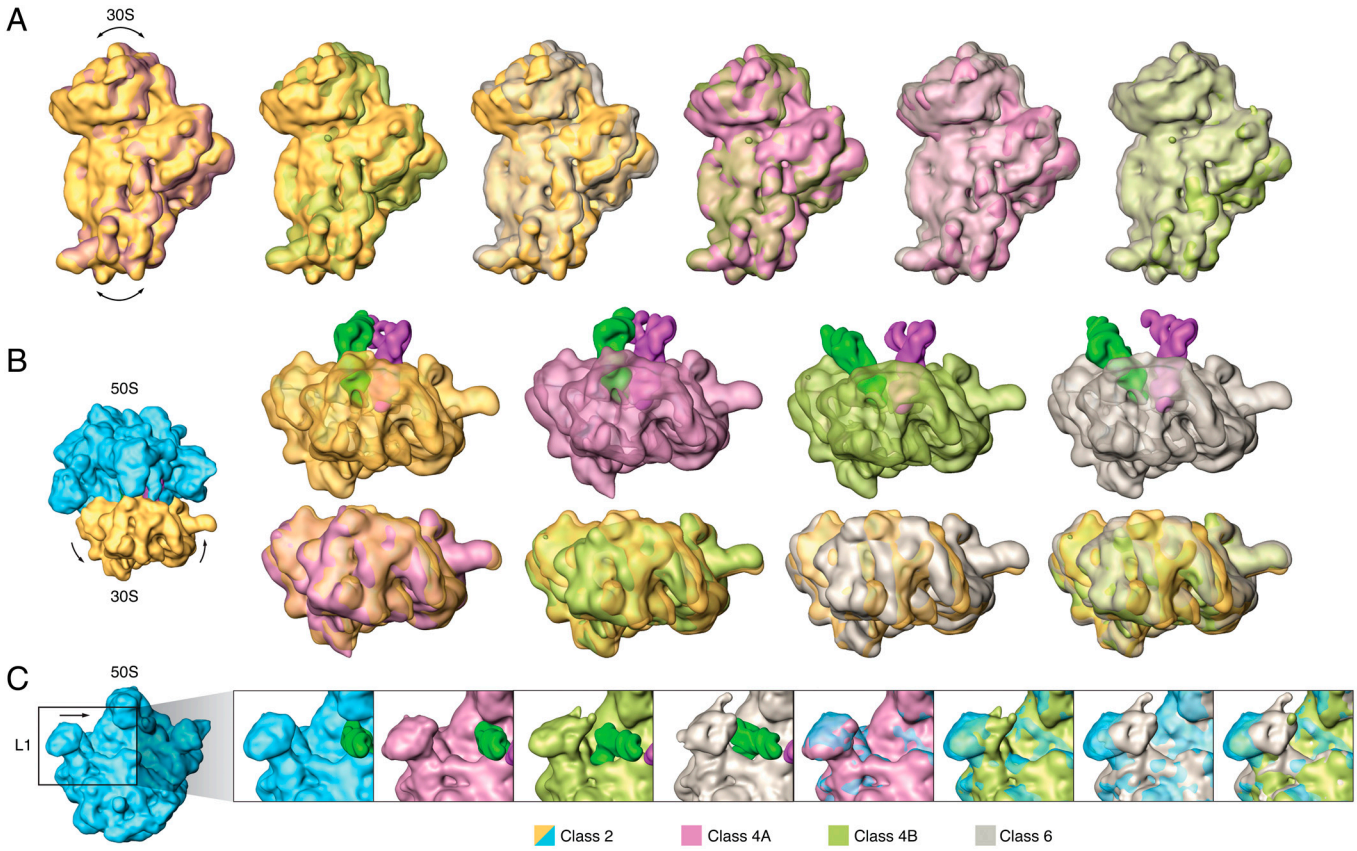

Fig. 1. Movement of domains and tRNAs. (*A*) Left to right, different superimposed cryo-EM densities of the 30S subunits from class 2 (yellow), class 4A (violet), class 4B (olive), and class 6 (gray). (*B*) Left to right, different reconstructions (upper row) and superimposed densities (lower row) of the 30S subunits; color-coded as in (*A*). The new orientation of the subunit is shown as a thumbnail on the left. The A- and P-site tRNAs are in magenta and green. (*C*) Left to right, close-ups of different reconstructions and superimposed cryo-EM densities of the 50S subunits; color-coded as in (*A*) and (*B*). The orientation of the subunits is shown as a thumbnail on the left. The arrows in (*A*), (*B*), and (*C*) indicate the directions of intersubunit rotation, head swivel, and L1 stalk movement, respectively. Colored labels identify the different class reconstructions.

Progression of Ribosomal Dynamics and tRNA Movements. When analyzing the structural movements implicated in tRNA translocation, including intersubunit rotation (Fig. 1*A*), swivelling of head domain (Fig. 1*B*), and inward movement of L1 stalk (Fig. 1*C*), a progression is seen as we go from class 2 (unrotated, classic state) over classes 4A and 4B to classes 5 and 6 (fully rotated, hybrid). Thus the new classes 4A and 4B represent two distinct structural intermediates during the first phase of translocation. While class 4A still shows classical-like tRNA positions, it displays distinct positions in the intersubunit rotation and L1 stalk movement. Class 4B is further along in both movements, and in addition shows a unique hybrid-like tRNA configuration: the deacylated P-site tRNA contacts the large subunit's E-site region via the acceptor stem, but it shows a distinct position of the elbow, approximately halfway through its transition from class 2 to classes 5 and 6.

To gain further insights, atomic models were built using MD-based flexible fitting (MDFF) as previously described (34). Movies S1 and S2 depict the conformational transitions between classes 2, 4B, and 6 by interpolation of the atomic coordinates generated for each of these classes, and represent (in this simplified model) a feasible pathway for forward translocation. Note that recent X-ray data show the reconfiguration of the intersubunit bridges that link the ribosomal subunits during the transition from the unrotated, classical to the rotated, hybrid state (35, 36). It may be possible to analyze the rearrangements of bridges, notably B1b (4), during the intermediate transitions by comparing the fitted structures in atomic detail, but the current resolution does not support a detailed fitting in the intersubunit region, as the gradients in the interface region distort the structure.

Atomic models generated for the tRNAs (Fig. 2; also see Fig. S4) show that, coupled to the intersubunit rotation, the P-site tRNA ASL-mRNA complex has moved laterally for class 4B and classes 5 and 6 compared to its position in class 2. In addition to the intersubunit rotation, a concomitant lateral movement of the tip of h44 with respect to its classical position is responsible for the shift in the A-site tRNA. In both fully classical and fully hybrid states (i.e., MS I and II), the A-site tRNA interacts with H69 and H38 via its D stem and its T arm, respectively. A slight reorientation of the ASL and elbow region, coupled with the straightening of the AS, is responsible for placing the CCA end of the A-site tRNA in the vicinity of the P site of the peptidyl-transferase center (PTC) in classes 5 and 6. In contrast, ribosomes in class 4B display the A/A configuration, although the location of the 3′ CCA end cannot be assigned unequivocally. As to the hybrid-like P/E-configuration tRNA, it is characterized in both intermediate (class 4B) and fully hybrid (classes 5 and 6) states by (*i*) a distortion in the vicinity of the ASL, enabling it to reach the E site with its 3′ end, and (*ii*) by loss of contact with H69. However, while going in the same direction, the magnitude of the rotation of the anticodon region is smaller for the new class-4B hybrid-like intermediate; this results in a different elbow position when compared to classes 5 and 6. Note that the acceptor stem of the hybrid-like P/E tRNA model in class 4B appears contracted, but it fits the density well.

Regarding the L1 stalk, we observe different conformations that are apparently coupled with the intersubunit rotation and—except for class 4A—changes in tRNA positions (see Fig. 1*C* and Fig. S4). In class 2, the L1 stalk is fully open. Classes 4A and 4B show (slightly distinct) intermediate positions for the L1 stalk

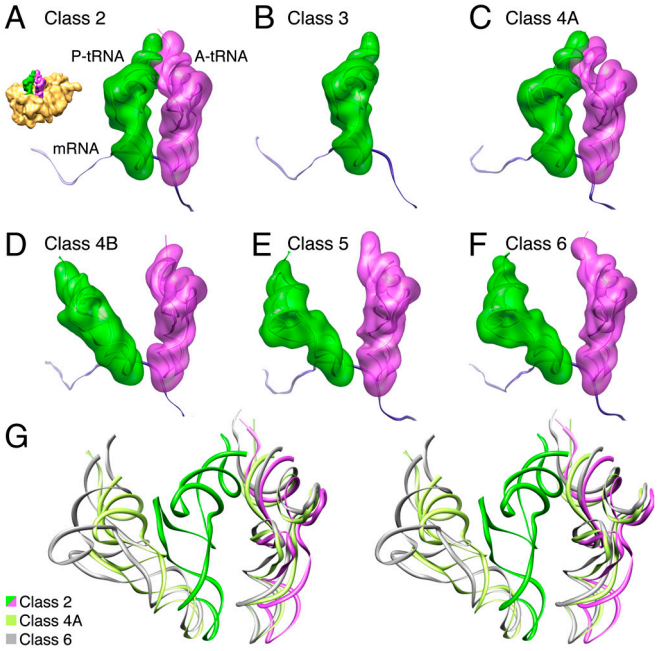

Fig. 2. Atomic models of tRNA obtained by flexible fitting. A gallery of images is shown for tRNA-mRNA complexes for classes as indicated in (*A*)–(*F*). Thumbnail in (*A*) shows the orientation of the tRNAs with respect to the 30S subunit (yellow). Cryo-EM densities for A- and P-site tRNAs are in transparent magenta and green. Fitted structures are in ribbons. Modeled mRNA sequence is shown in blue. (*G*) Stereo-views of fitted A and P-site tRNAs from class 2 (magenta and green), class 4B (olive), and class 6 (gray), aligned with respect to the 70S ribosomes (see colored labels). See also Fig. S4.

(class 4A being more proximal to the open position). Finally, classes 5 and 6 present a fully closed stalk along with the fully hybrid tRNA configurations and a fully rotated 30S subunit. A similar half-closed intermediate configuration of the L1 stalk as in class 4B was recently proposed on the grounds of smFRET analysis [see (22)] in the posttranslocational (POST) ribosome, which apparently presented E/E tRNAs and a nonrotated small subunit. We also note that in the analysis of the back-translocation process by Fischer and coworkers (29), only three L1 positions were found (open and closed in PRE complexes, half-closed in POST complexes), which may indicate that our class-4A and -4B intermediates are not visited during back-translocation, and that the two processes follow different preferred pathways. On the other hand, examination of the reconstructions shows that the L1 stalk does not participate in the stabilization of the class-4B intermediate hybrid position of the P/E tRNA, as it does for classes 5 and 6. However, due to the possibility that class 4B might contain some residual contamination as a consequence of merging particles from other classes—potentially some from classes 5 and 6 (see Fig. S2 for details)—it is still uncertain whether the new intermediate tRNA position is achieved independently of the action of the L1 stalk.

Quantification of Conformational Changes. To quantify the relative movements among the structures derived from the conformational classes, the displacement angles and distances for each structural feature relative to a reference structure were determined by tensor analysis (33). Tables S2 and S3 show the angles formed between selected vectors of the inertia tensors from two different components [for definition of angles between domains, see Suppl. Fig. 4 in Ref. (33)]. In addition, the different values in Table S4 track the progress of the tRNAs through the intersubunit corridor and the gradual closing of the L1 stalk. As the tRNAs travel through the ribosome, from the entrance to the exit of intersubunit space, we follow their movements by measuring the distances of their centers of mass (COMs) with respect to the COM of the very first tRNA; i.e., the A/A as manifest in class 2. The approach of measuring distances between centers of mass of a large selection of atoms was taken because distances between individual atoms, especially in the peripheral part, can be quite noisy, given the moderate resolution and the resulting fitting uncertainty. (The same approximation was taken in the tensor analysis that resulted in the rotation angles shown in Table S2 and S3).

Specifically, Table S2 contains quantitative descriptions of the movements of different ribosomal domains within the 30S subunit, as well as those of the L1 stalk and the tRNAs. In extending the analysis, Table S3 contains data describing relevant, published structures and include the X-ray crystal structures of 70S ribosomes in the presence of ASL tRNA mimics (31), which revealed intermediate states of intersubunit rotation (see 3I1Q-3I1R and 3I1Z-3I2O). PDB entries 2WRI-2WRJ and 2WRK-2WRL correspond to ribosome-EF-G complexes reported by X-ray crystallography (37). These structures, arrested in the POST state by fusidic acid, display no intersubunit rotation. On the other hand, the cryo-EM structures of ribosome-EF-G complexes obtained by Spahn and coworkers using image sorting (8), also in the presence of fusidic acid, display intersubunit rotation uncoupled to swiveling movements, and are considered PRE (2XSY-2XTG) and POST (2XUY-2XUX) states, respectively. The recently described structures of fully rotated ribosomes bound to RRF (35) are also included in the analysis (3R8N-3R8S and 3R8O-3R8T for rotated/hybrid and unrotated/classical ribosomes, respectively). Finally, the structures denoted as NR, IRS1, IRS2, and RS correspond to the nonrotated, the intermediate rotated structures 1 and 2, and the rotated structures, respectively, as obtained by cryo-EM of PRE complexes of mutant ribosomes (30).

From the analysis, it can be concluded that the cryo-EM structures 2XSY-2XTG and X-ray structures 3R8N-3R8S, obtained in the presence of RRF, most closely resemble our classes 5 and 6, while the structure 2XUY-2XUX is a state which we do not observe, characterized by a large swiveling angle of the head. In the latter structure, the tRNA is in fact more similar to the classical E/E tRNA than to a hybrid P/E tRNA. The X-ray crystal structures of 70S ribosomes in the presence of ASL tRNA mimics (31) are very similar to our class-4B reconstruction with regards to the intersubunit rotation. Note that the structure described by PDB entry 3I1M (31) also shows a considerable degree of swiveling of the head, although still falling short when compared to structure 2XUY-2XUX. On the other hand, when considering the body/platform opening values in hybrid forms, the structures can be divided in two groups: (*i*) the present cryo-EM structures and the X-ray structures obtained in the presence of ASL mimics and (*ii*) the hybrid structures obtained in the presence of EF-G (2XUY-2XUX, 2XSY- 2XTG) or RRF (3R8N-3R8S). We also note that structure 2XUY-2XUX shows a distinctive position of the head relative to the shoulder, as well as a strong tilt of the head domain toward the subunit interface. Structure 3I1M, and, to a lesser extent, the hybrid cryo-EM classes 5 and 6 show a similar trend, although the magnitude of the movement is less pronounced.

Of special interest are measurements for the structures obtained by Fu et al. (30). This work, a follow-up analysis of a smFRET study of P-loop mutant ribosomes (28), also described two intermediate states. We applied our tensor analysis to unpublished RSREF-fitted coordinates for these maps and observed that, as a function of intersubunit rotation, all domain movements show the same trends as in the current models, with the exception of the tilt of the small subunit head domain toward the subunit interface. A large difference is only seen in the position of the acceptor stem of the P-site tRNA for both IRS1 and IRS2, presumably the position most affected by the mutation. In terms of ribosome conformation alone, including intersubunit angle, IRS1 evidently corresponds to class 4A, and IRS2 to class 4B.

(RSREF-fittings for the A-site tRNA were not considered in this comparison as they show large inconsistencies).

Finally, we note that several X-ray structures of unrotated ribosomes in our table show intersubunit rotation angles that are smaller than those for our EM reconstructions of unrotated complexes. This could be explained by the uncertainty of classification in the EM data analysis, which may allow "adjacent" populations with larger rotation to contribute to our reconstructions. However, some X-ray structures even show negative values; i.e., less rotated than 2I2U/2I2V (38), the structure that was used as reference. Thus, it is possible that the subunit position is influenced by crystal packing effects or uncontrolled experimental effects (e.g., buffer conditions and temperature).

Coordination of the Dynamics Between the Ribosome and the tRNAs. We followed the way angles or distances of ribosomal components change as we move through the states, ordered according to "time" parameterized by intersubunit rotation. The rationale in singling out intersubunit rotation as an "independent" variable is that the movements of the massive subunits are likely to occur on a timescale that is considerably longer compared to the movements of all subunit domains and especially the tRNA. We envision that, being on a longer timescale, subunit positions will define the environment for the tRNAs, and thus dictate the range of domain and tRNA motions within energetic reach at any point in time. We therefore plotted the different measurements (ordinates) from Tables S2, S3, and S4 against the angle of intersubunit rotation (abscissa). Connecting lines between measurements have a meaning since they indicate, via interpolation, an estimate of where a given measurement would be if we had been able to sample the states more finely. We interpret the states with intermediate intersubunit rotations as intermediates in the transition of the ribosome from the classical to the final, fully rotated configuration.

To investigate the degree to which the movements of structural components are coupled, we also computed the correlation coefficients between all pairs of variables shown in Tables S2, S3, and S4 (see Fig. S6). These coefficients measure how closely any two variables are tied to each other by a linear relationship. Although causal relations cannot be proven based on correlation coefficients, a high correlation between quantities that measure the varying positions of ribosome components (notably L1 stalk versus intersubunit rotation, see below) indicates that we observe the gradual change of an entire tightly connected structure through different states.

Fig. 3*A* displays the trends of several angles measured on the small subunit in graphic form, while the progression of the L1 stalk closing and movement of tRNAs is displayed in Fig. 3 *B*–*E*. As seen in Fig. 3*A*, the intersubunit rotation occurs in concert with structural rearrangements within the 30S subunit. The closing of the body and platform runs through a maximum for the intermediate classes 4A and 4B. This is in qualitative agreement with the classical as well as partially (31) and fully rotated (35)

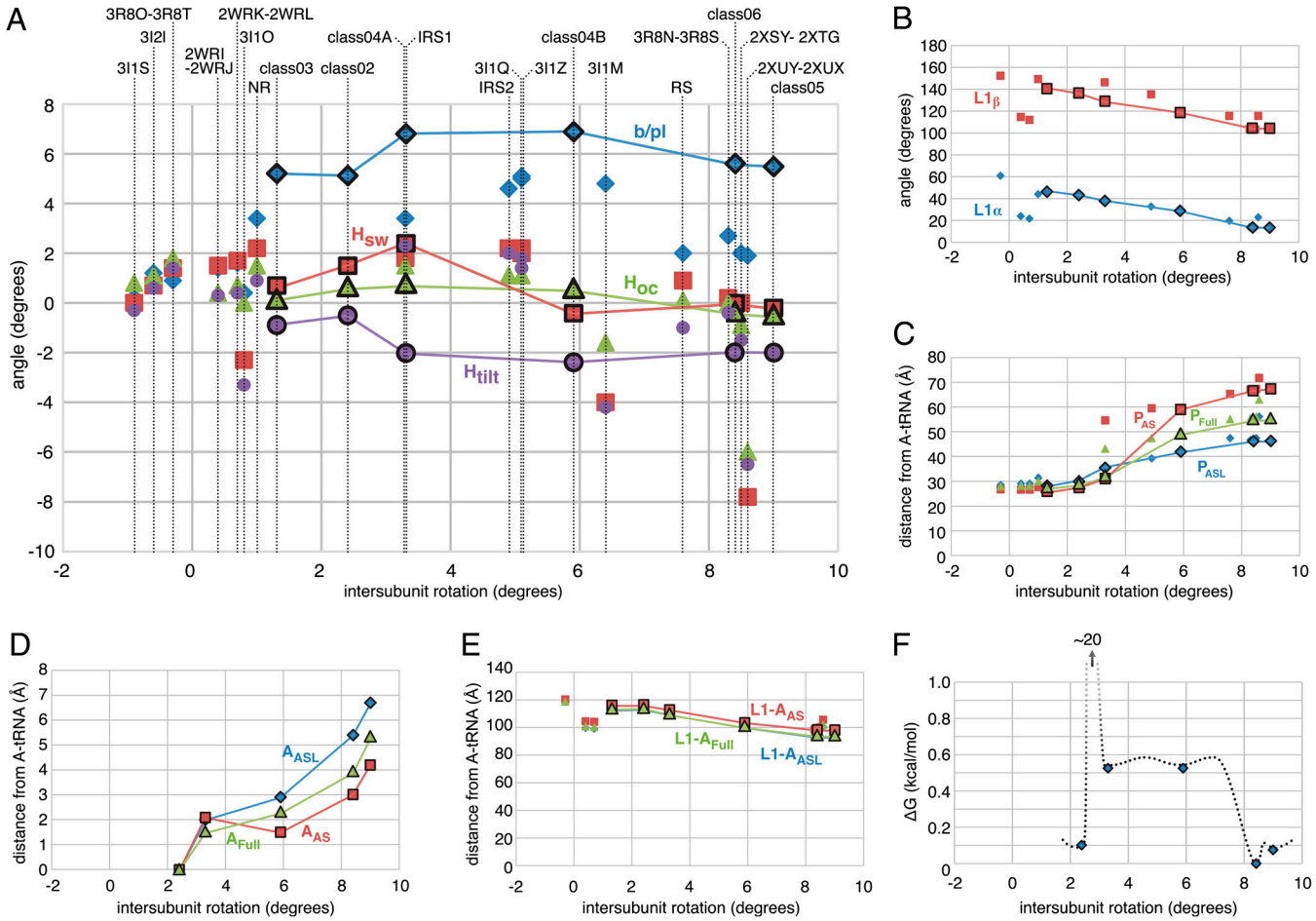

Fig. 3. Tensor analysis of individual domains. (*A*) Trends of measured angles on the small subunit for this study (connected points), those obtained by Fu et al. (32) (NR, IRS1, IRS2, RS) and those by X-ray crystallography (PDB codes indicated). The values plotted, b/pl, H_{tilt}, H_{oc}, and H_{sw}, are as defined in Tables S2 and S3. (*B*) Progression of the L1 stalk closing. ($L1_\alpha$ and $L1_\beta$ correspond to the same angle in an oblique plane). (*C*, *D*, *E*) Progression of tRNA and L1 movements. (*F*) Free-energy landscape along the intersubunit rotation coordinate, computed from occupancies of states in equilibrium. The numbers describe the relative stabilities of the various ground states. Dotted line represents the largely unknown topology of the energy landscape between the sample points obtained by cryo-EM. It includes a peak at 20 kcal/mol, going off scale in our diagram, indicating the barrier separating MS I and MS II as calculated from tRNA-tRNA smFRET measurements.

structures obtained by X-ray crystallography; note that the apo forms (31IO and 31IM) behave differently due to the lack of tRNAs. A very similar behavior can be observed for the closing of the head domain relative to the shoulder of the 30S subunit and the tilt of the head with respect to the subunit interface. However, while the motion relative to the shoulder closes the small subunit during the rotation, a larger rotation goes along with a tilt of the head away from the interface. The latter observation may be rationalized by the potential strain caused by the P-site tRNA moving between the head and the apical part of h44. However, the crystal structures of partially rotated ribosomes show a larger tilt *toward* the interface for tRNA-containing complexes, while a large tilt *away* from the interface is observed for the apo form. The origin of this discrepancy is not clear. A somewhat different trend is observed for the swiveling of the head domain: the head rotates away from the subunit interface reaching the maximum amplitude at class 4A and rotates back subsequently. This behavior can be observed in X-ray crystal structures (31, 35). Interestingly, however, the partially rotated structures of the ribosome in complex with tRNAs shows larger swiveling, while the apo complex shows significantly smaller swiveling than presently observed. Obviously, the presence of tRNAs does not allow the head domain to rotate too far into the intersubunit space. Note that the head already swivels back at the point when the body and platform are still closed and the head domain is closed relative to the shoulder (class 4B).

One of the most striking observations in the graphs is that the motion of the L1 stalk as a function of intersubunit rotation is reflected by a strict (negative) proportionality between stalk and intersubunit angles (Fig. 3*B*). The rationale for the high correlation may be found in the normal-mode analysis by Tama and coworkers (39), who found these movements to be coupled in one of the principal modes of the mechanical system. The only outliers on this graph belong to data obtained by X-ray crystallography, presumably since the component is peripheral, and thus strongly affected by crystal contacts.

The progression of tRNA and L1 movements is shown in Fig. 3 *C*–*E*. For both tRNAs, a continuous progression is seen as the intersubunit rotation angle increases. The classic-to-hybrid transition is reflected in the motions of AS and ASL for A- and P-site tRNAs, as well as in the change of angle formed by the two arms of the tRNA. Looking at the angles characterizing the tRNA structures and constellations, it is now seen that classes 5 and 6, which are similar with regards to ribosomal conformation, are in fact slightly different as far as the tRNAs are concerned. In contrast to the P-site tRNA (panel 4*C*), the graphs B and E show anomalies in the X-ray measurements—they do not fit into the smooth trajectory of the EM data. In contrast, the reconstructions from Spahn and coworkers (8) fit into our data quite well. The correlation analysis (Table in Fig. S6) shows similar trends as the plots in Fig. 3. For example, the negative correlation between L1 stalk motion and intersubunit rotation is so high that it almost suggests the existence of a gear.

The analysis also reveals the participation of the head swiveling in the movement of the P-site tRNA [via A-minor interactions between the head and the P-site-tRNA ASL, see (31)]. Something similar may also go on in the case of the correlation between the A-site ASL and the opening/closing of the small subunit, as it is conceivable that the closing of the body "pushes" the tRNA. Interestingly, there is a strong correlation of the intersubunit rotation with the distance of the ASL of the A-site tRNA but not with the corresponding angle. Conversely, the opening/closing of body/platform is correlated with the angle, but not the distance, of the ASL of the A-site tRNA.

Translating Relative Occupancies of the PRE States into Free-Energy Differences. The classification has given us numbers of molecules in each state as a by-product of the analysis. In a freely equilibrating system, these numbers reflect relative stabilities of the corresponding states, and can be converted into free-energy differences ΔG, reflecting the topology of the energy landscape (18, 19, 29). In this conversion we followed the analysis by Fischer et al. (29) (see *Supporting Information*). We take the energetics of the intersubunit rotation as the most interesting quantity to evaluate (see Fig. 3*F*), even though similar plots can be obtained for any of the quantities measured and tabulated in Tables 1–3.

Evidently (Fig. 3*F*), the intermediate states represented by classes 4A and 4B are energetically unfavorable relative to classes 2, 5, and 6, representing local minima within a relatively flat, plateau-like barrier that molecules traversing from the MS I ground state (class 2) to the MS II ground state (classes 5 and 6) must cover. According to the calculated landscape, the lowest free-energy minimum appears at the position of the hybrid, fully rotated forms, in line with FRET experiments showing that excursions to the classical state are less likely under the given experimental conditions (40). From the analysis, it can be concluded that classes 4A+4B and 5+6 represent two "superstates," the latter corresponding to MS II. In both cases, the energy minima of the constituent states are closely matched, suggesting local equilibration in the corresponding regions of the energy landscape.

Discussion

As shown by our work, the ribosome PRE complex exists as an ensemble of substates which span a large conformational space. Understanding the correlated dynamics of this system is essential for mapping structure to function. To this end, we have studied the multidimensional range of conformations sampled by the ribosome, by combining cryo-EM and MD techniques with the quantification of domains rearrangements. Our premise has been that extending the analysis to include correlations among movements of subunit domains and tRNAs contributes to defining the framework of functional interactions within the translating ribosome. Among other unresolved questions, the results of our study may contribute to the discussion concerning temporal uncoupling between movements of tRNA and the L1 stalk on the one hand (41) and between movements of the L1 stalk and intersubunit rotation on the other, as suggested by smFRET (22).

There is also currently a debate over the extent to which intermediates are sampled in wild-type PRE ribosomes during translocation. For example, a recent tRNA-tRNA smFRET study (26) found no evidence for intermediates in WT ribosomes, even when employing hidden Markov modeling methods similar to those used in Munro et al. (28). All existing crystallographic and cryo-EM studies that identified intermediate structures of ribosome-tRNA complexes used mutant ribosomes, ASL mimics, an empty A site or other modifications that impair or prohibit translocation. To date, our study is the only one to identify intermediate states of a PRE ribosome-tRNA complex, prepared using WT bacterial ribosomes and intact tRNAs, and competent for unimpaired forward translocation.

The observation of a progression in movements of structural components and tRNAs in our study suggests that the PRE ribosome oscillates between two extreme conformations going through at least two intermediates with distinct conformations. It is in the nature of such pathway intermediates that they represent stepping stones without commitment of the molecule to proceed further in the same direction; i.e., ribosomes captured in classes 4A and 4B may either be on pathway from one extreme to the other, or represent unsuccessful attempts of a ribosome in the MS-I or MS-II state to acquire the alternative end conformation. On the other hand, since in cryo-EM we only "see" molecules that occur in sufficient numbers, settled in local minima, the actual profile of the free-energy landscape is expected to be more complex (e.g., as suggested by a dotted line in Fig. 3*F*), but its trajectory outside the minima is only accessible by alternative experimental methods, such as smFRET (18, 19). In this context we

note that for simplicity, Movies S1 and S2 display the conformational changes as a single, continuous, unidirectional process; in reality the changes are discontinuous, with long "pauses" in the wells, and—as the true free-energy landscape is likely very complex—multiple pathways connecting the observed conformational states may exist.

The calculated free-energy landscape suggests that all observed states are interchangeable, with little energetic difference (<1 kcal/mol). In contrast, smFRET studies report that the activation energy required to initiate the movement of the 30S subunit rotation from one macrostate to the other is considerably larger, in the order of 20 kcal/mol (12, 19). It is tempting to suggest that the required reconfiguration of intersubunit bridges, notably those in the periphery of the intersubunit space (4, 35, 36) presents the activation barrier, with one or more poorly occupied, short-lived high-energy transition states, unlikely to be captured by cryo-EM. As to the location of the barrier on our free-energy plot, a plausible placement is at the very beginning of the intersubunit rotation (Fig. 3*F*), where proteins L5 and S13, the two components of intersubunit bridge B1b, are locked by juxtaposition of opposing charges (4). Additional free-energy barriers may exist in the whole range.

All in all, our data support the idea that the intersubunit motion necessary for translocation occurs in several steps, and that each step involves a conformational reorganization of the ribosome and each of its subunits. These changes determine the corresponding configurations of the tRNAs. The progression we see implies that the different motions are coupled, if not kinetically then certainly thermodynamically. Evidently, the intermediate steps of incremental conformational changes and mRNA/tRNA binding positions are necessary to ensure processivity during translocation, as the binding partners are not allowed to disengage from the ribosome, and we can assume that all other phases of translation follow the same principle.

Note: As this manuscript was finalized, we became aware of a study of the PRE mammalian ribosome with the same methods of cryo-EM and classification (42). The results of this study, including the existence of intermediate positions of the tRNAs, are in broad agreement with our study of the *E. coli* system.

Materials and Methods

Image Processing. The ribosomal complex was prepared as described (15). To separate the heterogeneous dataset into structurally homogeneous subsets, a maximum-likelihood (ML)-based classification approach (32), was applied (see *SI Methods*).

Fitting of Crystallographic Structures into Electron Microscopy Densities. Structural models for the different conformational states of the ribosome were obtained using MDFF (34) (see *SI Methods*).

ACKNOWLEDGMENTS. We thank Ruben L. Gonzalez for a critical reading of the manuscript, Melissa Thomas for assistance with the preparation of the illustrations, and Wen Li for assistance with the deposition of the atomic models. X.A. is a recipient of a "Ramon y Cajal" fellowship from the Spanish Government (RYC-2009-04885). Supported by Grant PI2011-23 from the Department of Education, Universities and Research of the Basque Country (to X.A.), Howard Hughes Medical Institute and National Institutes of Health Grants R01 GM55440 and R37 GM29169 (to J.F.), National Institutes of Health Grant R01 GM059425 (to R.G.), and National Institutes of Health P41-RR005969 and National Science Foundation PHY0822613 (to K.S). Computer time for MDFF simulations was provided by National Science Foundation through the National Resources Allocation Committee (MCA93S028).

1. Spirin AS (1968) How does the ribosome work? A hypothesis based on the two subunit construction of the ribosome. *Curr Mod Biol* 2:115–127.
2. Bretscher MS (1968) Translocation in protein synthesis: A hybrid structure model. *Nature* 218:675–677.
3. Agirrezabala X, Frank J (2009) Elongation in translation as a dynamic interaction among the ribosome, tRNA, and elongation factors EF-G and EF-Tu. *Q Rev Biophys* 42:159–200.
4. Frank J, Gao H, Sengupta J, Gao N, Taylor DJ (2007) The process of mRNA-tRNA translocation. *Proc Natl Acad Sci USA* 104:19671–19678.
5. Moazed D, Noller HF (1989) Intermediate states in the movement of transfer RNA in the ribosome. *Nature* 342:142–148.
6. Frank J, Agrawal RK (2000) A ratchet-like inter-subunit reorganization of the ribosome during translocation. *Nature* 406:318–322.
7. Schuwirth BS, et al. (2005) Structures of the bacterial ribosome at 3.5 A resolution. *Science* 310:827–834.
8. Ratje AH, et al. (2010) Head swivel on the ribosome facilitates translocation by means of intra-subunit tRNA hybrid sites. *Nature* 468:713–716.
9. Taylor DJ, et al. (2007) Structures of modified eEF2 80S ribosome complexes reveal the role of GTP hydrolysis in translocation. *EMBO J* 26:2421–2431.
10. Spahn CM, et al. (2004) Domain movements of elongation factor eEF2 and the eukaryotic 80S ribosome facilitate tRNA translocation. *EMBO J* 23:1008–1019.
11. Julian P, et al. (2008) Structure of ratcheted ribosomes with tRNAs in hybrid states. *Proc Natl Acad Sci USA* 105:16924–16927.
12. Blanchard SC, Kim HD, Gonzalez RL, Jr., Puglisi JD, Chu S (2004) tRNA dynamics on the ribosome during translation. *Proc Natl Acad Sci USA* 101:12893–12898.
13. Fei J, Kosuri P, MacDougall DD, Gonzalez RL, Jr. (2008) Coupling of ribosomal L1 stalk and tRNA dynamics during translation elongation. *Mol Cell* 30:348–359.
14. Cornish PV, Ermolenko DN, Noller HF, Ha T (2008) Spontaneous intersubunit rotation in single ribosomes. *Mol Cell* 30:578–588.
15. Agirrezabala X, et al. (2008) Visualization of the hybrid state of tRNA binding promoted by spontaneous ratcheting of the ribosome. *Mol Cell* 32:190–197.
16. Ermolenko DN, et al. (2007) Observation of intersubunit movement of the ribosome in solution using FRET. *J Mol Biol* 370:530–540.
17. Spirin AS (2009) The ribosome as a conveying thermal ratchet machine. *J Biol Chem* 284:21103–21119.
18. Munro JB, Sanbonmatsu KY, Spahn CM, Blanchard SC (2009) Navigating the ribosome's metastable energy landscape. *Trends Biochem Sci* 34:390–400.
19. Frank J, Gonzalez RL, Jr. (2010) Structure and dynamics of a processive Brownian motor: The translating ribosome. *Annu Rev Biochem* 79:381–412.
20. Pan D, Kirillov SV, Cooperman BS (2007) Kinetically competent intermediates in the translocation step of protein synthesis. *Mol Cell* 25:519–529.
21. Fei J, et al. (2009) Allosteric collaboration between elongation factor G and the ribosomal L1 stalk directs tRNA movements during translation. *Proc Natl Acad Sci USA* 106:15702–15707.
22. Cornish PV, et al. (2009) Following movement of the L1 stalk between three functional states in single ribosomes. *Proc Natl Acad Sci USA* 106:2571–2576.
23. Munro JB, Altman RB, Tung CS, Sanbonmatsu KY, Blanchard SC (2010) A fast dynamic mode of the EF-G-bound ribosome. *EMBO J* 29:770–781.
24. Munro JB, Wasserman MR, Altman RB, Wang L, Blanchard SC (2010) Correlated conformational events in EF-G and the ribosome regulate translocation. *Nat Struct Mol Biol* 17:1470–1477.
25. Ermolenko DN, Noller HF (2011) mRNA translocation occurs during the second step of ribosomal intersubunit rotation. *Nat Struct Mol Biol* 18:457–462.
26. Chen C, et al. (2011) Single-molecule fluorescence measurements of ribosomal translocation dynamics. *Mol Cell* 42:367–377.
27. Ermolenko DN, et al. (2007) The antibiotic viomycin traps the ribosome in an intermediate state of translocation. *Nat Struct Mol Biol* 14:493–497.
28. Munro JB, Altman RB, O'Connor N, Blanchard SC (2007) Identification of two distinct hybrid state intermediates on the ribosome. *Mol Cell* 25:505–517.
29. Fischer N, Konevega AL, Wintermeyer W, Rodnina MV, Stark H (2010) Ribosome dynamics and tRNA movement by time-resolved electron cryomicroscopy. *Nature* 466:329–333.
30. Fu J, Munro JB, Blanchard SC, Frank J (2011) Cryoelectron microscopy structures of the ribosome complex in intermediate states during tRNA translocation. *Proc Natl Acad Sci USA* 108:4817–4821.
31. Zhang W, Dunkle JA, Cate JH (2009) Structures of the ribosome in intermediate states of ratcheting. *Science* 325:1014–1017.
32. Scheres SH, et al. (2007) Disentangling conformational states of macromolecules in 3D-EM through likelihood optimization. *Nat Methods* 4:27–29.
33. Agirrezabala X, et al. (2011) Structural insights into cognate versus near-cognate discrimination during decoding. *EMBO J* 30:1497–1507.
34. Trabuco LG, Villa E, Mitra K, Frank J, Schulten K (2008) Flexible fitting of atomic structures into electron microscopy maps using molecular dynamics. *Structure* 16:673–683.
35. Dunkle JA, et al. (2011) Structures of the bacterial ribosome in classical and hybrid states of tRNA binding. *Science* 332:981–984.
36. Jin H, Kelley AC, Ramakrishnan V (2011) Crystal structure of the hybrid state of ribosome in complex with the guanosine triphosphatase release factor 3. *Proc Natl Acad Sci USA* 108:15798–15803.
37. Gao YG, et al. (2009) The structure of the ribosome with elongation factor G trapped in the posttranslocational state. *Science* 326:694–699.
38. Berk V, Zhang W, Pai RD, Cate JH (2006) Structural basis for mRNA and tRNA positioning on the ribosome. *Proc Natl Acad Sci USA* 103:15830–15834.
39. Tama F, Valle M, Frank J, Brooks CL, 3rd (2003) Dynamic reorganization of the functionally active ribosome explored by normal mode analysis and cryo-electron microscopy. *Proc Natl Acad Sci USA* 100:9319–9323.
40. Kim HD, Puglisi JD, Chu S (2007) Fluctuations of transfer RNAs between classical and hybrid states. *Biophys J* 93:3575–3582.
41. Munro JB, et al. (2010) Spontaneous formation of the unlocked state of the ribosome is a multistep process. *Proc Natl Acad Sci USA* 107:709–714.
42. Budkevich T, et al. (2011) Structure and dynamics of the Mammalian ribosomal pretranslocation complex. *Mol Cell* 44:214–224.